In-Band Full-Duplex Signal Interference Monitoring Technology

Toyoyuki Kato, Takashi Mori, Masanori Takizawa, Takashi Kawamura, Yuichi Maruyama

[Summary] Growth of mobile traffic continues to increase due to the recent spread of smartphones and mobile UE as well as expanded capacity and faster speeds of wireless communications systems, resulting in routine congestion of frequency bands. To solve this issue, the Japanese Ministry of Internal Affairs and Communications (MIC) started R&D from 2005 into expansion of radio-wave resources to develop new frequency bands, promote joint frequency use, and improve frequency usage efficiency. As part of this program, Anritsu Corporation started R&D for 4 years from 2019 into in-band full-duplex signal interference monitoring technology. This article outlines in-band full-duplex communications and reports on a prototype of monitoring system for monitoring and analyzing interference data.

1 Introduction

With the introduction of fifth generation (5G) mobile systems, although use of the super-high frequency (SHF) band is starting, the required number of channels cannot be secured and there are rather difficulties to find fundamental resolution for frequency band shortage. Additionally, although various technologies, such as Multiple Input Multiple Output (MIMO) and Non-Orthogonal Multiple Access (NOMA), etc., are being researched and implemented to improve frequency usage efficiency, still further increases in mobile traffic are forecast and more improvements to frequency usage efficiency are expected. Research and development into one candidate — in-band full-duplex (hereafter full-duplex) is progressing, and Anritsu is researching interference monitoring required to implement this full-duplex technology.

Section 2 of this article describes full-duplex technology first, followed by section 3 outlining interference monitoring technology, and section 4 explaining the developed interference monitoring equipment.

2 In-band Full-Duplex

Conventional mobile communications systems generally use either time division duplex technology (TDD) in which sending and receiving between base stations (hereafter BS) and user terminals (hereafter UE) is time divided, or frequency division duplex technology (FDD) in which communications are divided by frequency. In the TDD technology with superior frequency usage efficiency (Figure 1a) downlink (DL) sending from the BTS to the UE, and uplink (UL) sending from the UE to the BTS use the same frequency but are run pseudo simultaneous communications in time divided. In contrast, by using the full-duplex (Figure 1b) technology, multiple UE which are affected no interference run sending and receiving in the same time slot and same frequency simultaneously.

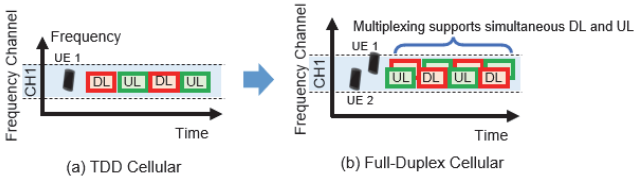

Figure 1 Difference Between TDD and Full-Duplex

Figure 2 shows an example of a full-duplex configuration single cell with one BS and two UE. Here the BS is simultaneously receiving a UL from UE#2 while sending a DL to UE#1. In this case, there is a risk of interference occurring between the UL from UE#2 to the BS and the DL from the BS to UE#1. One case of them is occurring it nearby the BS called self-interference (hereafter SI), and another case is occurring it nearby UE#1 called inter-UE interference (hereafter IUI). SI can be suppressed with self-interference cancellation function to be implemented in BS for removal of DL signal transmitted by BS own from received signal containing UL signal from UE. On the other hand, cancellation measures similar to those for BS are difficult to implement for IUI due to limited resources of UE, such as CPU power, memory amount, so-on. Consequently, the BS is to full-duplex communications with concerned UE limited only when the impact of IUI can be ignored.

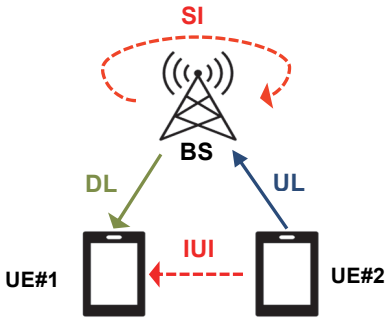

DL: Download, UL: Upload, BS: Base Station,
UE: User Equipment, SI: Self Interference, IUI: Inter-UE Interference

Figure 2 Full-duplex Communications

In the actual usage environment, there will be much more type of interference. Figure 3 shows the relationship between the mutual interference occurring between multiple adjacent cells. In the full-duplex cellular system, to cope with newly emerged interference (solid lines in Figure 3), signals are monitored and the degree of interference is analyzed to select a UE to apply full-duplex operation, as well as it suppresses suffered and emitting interference with control Tx timing and power according to the degree of interference.

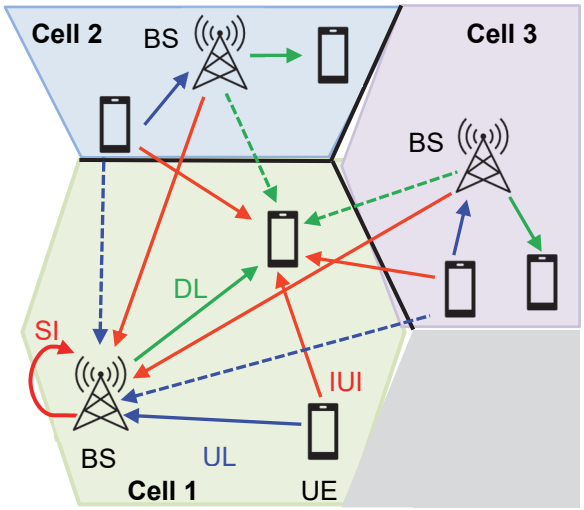

DL: Download, UL: Upload, BS: Base Station, UE: User Equipment,
SI: Self Interference, IUI: Inter-UE Interference

Previous interference
New interference caused by full-duplex

Figure 3 Full-Duplex Cellular System Interference Model

3 Interference Monitoring Technology

3.1 OFDMA Interference Monitoring Technology

The Orthogonal Frequency Division Multiple Access (OFDMA) technology used by 5G supports communications by allocating frequency and time slots in resource block (RB) units to each UE. Since explicit information for identifying the signal source is not included in the signal itself, it is not easy to separate multiple mixed signals. Interference monitoring technology measures the wireless signals emitted into free space from the several UE indicated by the dashed lines in Figure 3 and uses the information contained in the mixed OFDMA signals to separate the signals, to estimate the arrival direction of each signal and to analyze interference conditions. These functions are broadly divided into three. Figure 4 shows the structure.

(1) Antenna System for Estimating Space–Time Arrival Direction

Captures RF signals for monitoring difference between signal source physical position and transmission path due to use of multi-element antenna array.

(2) Multi-channel Receiver

Digitizes after down-converted multiple analog RF signals monitored by each element of antenna system and converts to data for blind signal estimation processing.

(3) Algorithm for Estimating Blind Signals

Estimates arrival direction from multiple signal sources using Blind Signal Separation method based on solving mixed model inversion matter.

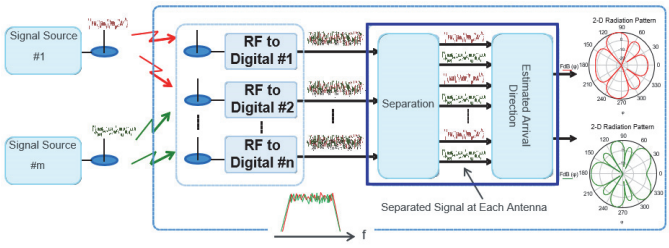

Figure 4 Interference Monitoring Function Configuration

3.2 Blind Signal Estimation Algorithm

We adopted algorithm based on Independent Component Analysis[10] (ICA)-which is widely used to detect blind signals for separating mixed multiple signals.

3.2.1 Signal Separation using FDICA

With the ICA, mixed signal are separated into original independent elements based upon assumption of signal sources independency. This method uses the central limit theorem that a mixed signal composed of a mixture of multiple signals approaches a Gaussian signal, but it obtains the estimated signal with minimum independence by minimizing the Gaussian characteristics of the mixed signal. Incidentally, since an OFDMA signal is multiplexed orthogonally

in the frequency domain and is scattered in multiple carriers, its signal amplitude has a Gaussian distribution in the time domain due to the central limit theorem (Figure 5 (a)). As a result, since ICA cannot be applied as is to OFDMA signals, Frequency Domain ICA (FDICA)[12), 13)] is used to obtain ICA in the frequency domain (Figure 5 (b)). FDICA applies complex-number ICA independently to each frequency bin of the monitored signal to estimate blind signals across all frequencies by separation matrix for each frequency. With the conversion to the frequency domain, the signal time translational would be expressed as phase drift to be possible to handle delay waves in a multi-path environment together at the same time. This has the advantage of cutting the number of antennas in comparison to handling separately.

InfoMax[17)] and FastICA[18)] are typical ICA methods. The former substitutes the issue of non-Gaussian maximization with the issue of maximization of the likelihood function and solves using the (natural) gradient method. The latter preprocesses the signal to limit the range and fast optimization with fixpoint method. FastICA was chosen this time because it does not require learning rate settings unlike InfoMax using the gradient method. Use of ICA for complex signals requires some precautions such as inputting the signal absolute value[19), 20)] at the contrast factor measuring the non-Gaussian characteristics of the separation signal to be not non-correlation between the real and imaginary parts.

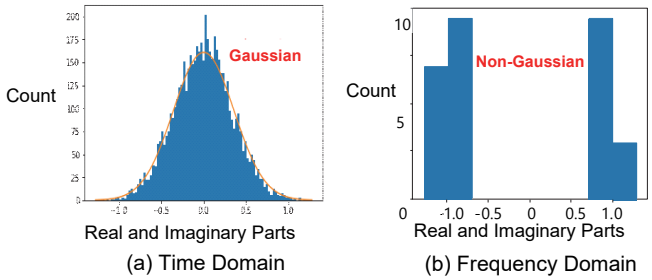

Figure 5 Frequency Distribution of Real and Imaginary Parts of OFDMA Signal

3.2.2 Component Separation and Reconfiguration using Clustering

FDICA is composed of Fourier transformation followed by two clustering stages to separate the components obtained by ICA. Clustering classifies the separation components for each signal source using some method in order to rebuild the signal sources using the separation components obtained by ICA for each frequency.

There are several separation component clustering methods[12), 13), 14), 15)]. To avoid making suppositions as far as possible here, we did not use the continuity[12), 14)] of the reference signal[13)] and the allocated signal frequency (sub-carrier) but instead used a method[15)] focusing on arrival of the same signal components from the same direction. This article presupposes use of a multi-path environment and rather than using the angle of arrival (hereafter AoA) of signal components[15)] itself, instead used angular spectrum (hereafter beam pattern) of the direction of arrival (hereafter DoA) obtained using the beamforming method[5)]. The MUltiple SIgnal Classification (MUSIC)[11)] method is a well-known as having a higher resolution than the beamforming method. However, because only single frequency components are obtained clearly in some frequency bins, the signals via multipath are completely correlated. Consequently, subspace methods, such as MUSIC, cannot be used to create FDICA clustering elements.

Signal beam patterns at the Rx side are obtained by applying the reverse projection method to the ICA results[21)] followed by the beamforming method. The power in each arrival direction $\theta \in \{-90, -89, \ldots, 90\}$ is treated as a point within $\mathbb{R}^{181}$ and clustering is performed. Typical candidate clustering methods are k means[22)], spectral clustering[23)], and hierarchical clustering[24)] (especially, single consolidation method here). Under multi-path environment, the shape of the beam pattern graph is anisotropic. Since the k means method assumes an isotropic cluster shape, we used the spectral clustering and single linkage method that can be applied to any cluster shape. These methods perform clustering by treating the data as a graph. In other words, a graph is configured by applying beam pattern as the peak, and length of its interpeak and degree of similarity as the sides. The similarity choice is critical with this kind of clustering. From the clustering viewpoint, it is better to use k-nearest neighbor graph made from the similarity of neighborhood points[23)] only in order to create a sparse graph.

4 Equipment Outline

We prototyped an equipment for purpose to study the interference monitoring technology. Table 1 lists the required specifications and main functions.

This prototype estimates the DoA using the interference monitoring process technology described in section 3.1 (1) to

(3) on OFDMA signals received by the antennas. The following sections introduce each part.

Table 1 Interference Monitoring Equipment Items and Required Specifications

Item	Specification/Function
Target Frequencies	Sub-6 GHz band (3.7 GHz, 4.5 GHz) SHF band (>28 GHz)
RBW	100 MHz
Estimated DoA Error	±10° max
Separated Signal Interference Suppression Ratio	10 dB max

4.1 Antenna System

We fabricated a sleeve antenna to estimate the arrival direction for both high-SHF band (28.2 to 29.1 GHz) and Sub-6 GHz band (3.75/4.65 GHz) signals. Figure 6 shows the external appearance and structure. In particular, this article introduces the high-SHF band array antenna.

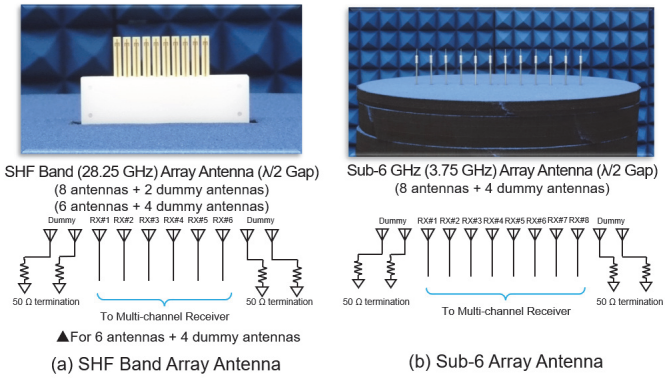

Figure 6 Antenna System

Since it is difficult to fabricate a high-SHF band antenna with coaxial cable as done it for Sub-6 GHz antenna from the perspectives of processing accuracy and mass production, we used a double-sided PCB to create a coaxial antenna like a Sub-6 GHz antenna. Due to the high frequency band and long feeder, we chose the MEGTRON7, R-5785(N) (Panasonic Industry) PCB material with low loss even at high frequency bands (3.4 dielectric constant; 0.002 dielectric tangent). Figure 7 shows the antenna configuration. In particular, to reduce reflections caused by a GND board for emitted waves, the antenna element feeder used a parallel flat line not requiring a GND board. The microstrip line on the left side of the PCB was converted to parallel flat line using a taper balun to connect to the sleeve antenna elements at the tip. Since the structure using both surface of the PCB causes tilt on the directivity of the perpendicular plane (E plane), metal pattern of the antenna is aggregated on the one side of the PCB, and used Via hole to connect to there.

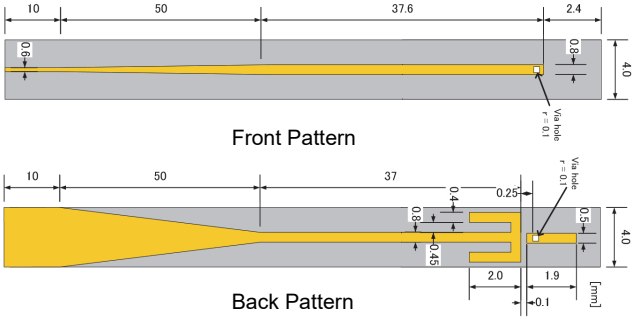

Figure 7 Two-Sided PC Board SHF-Band Sleeve Antenna

Figure 8 (a) shows the measured S_{11} results of the fabricated antenna. An S_{11} value of ≤−10 dB confirms sufficient antenna performance in the target 28.2 to 29.1 GHz frequency band. Figures 8 (b) and (c) show the typical measured directivity at a center frequency of 28.65 GHz in the used frequency band. The directivity level is normalized by the maximum value of the main polarized wave. Although there is ripple in the vertical directivity, since the level of the intersecting polarized waves is −15 dB at the same horizontal directivity, the fabricated antenna has sufficient performance for estimating the arrival direction.

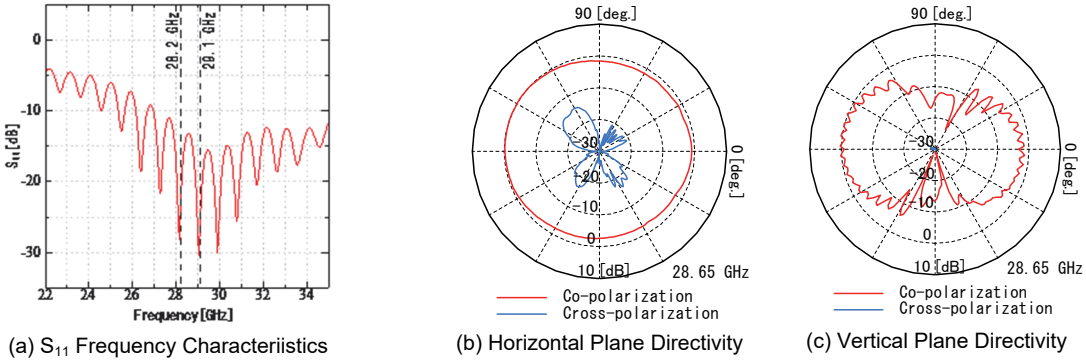

Figure 8 SHF-Band Sleeve Antenna Evaluation Results

4.2 Multi-channel Receiver

The multi-channel receiver has an RF section to down-convert a maximum of eight RF signal channels received by the array antenna to IF as well as a digital section to digitize these down-converted IF signals.

The RF section is a down-converter for the 8ch high-SHF and Sub-6 GHz bands; it helps achieve high resolution performance by using a low-phase-noise local signal. The input signal is an OFDMA QPSK/16QAM/64QAM/256QAM signal with a sub-carrier spacing of 30 to 120 kHz and a bandwidth of 100 MHz. The peak power is high compared to the average power and since the signal quality is degraded by non-linearity, the level diagram is created by taking this type of signal quality into consideration. The local signal source is designed by considering the phase noise caused by the narrow sub-carrier spacing. Since this equipment processes signals to estimate arrival direction based on inter-channel carrier phase difference, the delay time and phase of each channel must be aligned. Consequently, each channel uses the same local signal and is designed same configuration with the equal length wiring; phase error due to individual differences is held to within ±20° in the Sub-6 GHz band and to within ±90° in the high-SHF band. Software-based phase calibration is applied at the final stage.

4.3 Interference Monitoring Equipment

By integrating the antenna system (section 4.1) and the multichannel receiver (section 4.2) described above and incorporating the signal estimation algorithm (section 3.2), we prototyped an interference monitoring equipment that supports the high SHF band and the Sub-6 GHz band. Figure 9 shows the block configuration and Figure 10 shows the external view. The configuration at high-SHF band measurement uses the antenna shown in Figure 6 (a) connects dedicated down-converter module to convert from the high-SHF band to IF. Similarly, the Sub-6 GHz band measurement uses the array antenna shown in Figure 6 (b) with down-converter in the RF section converting from the Sub-6 GHz band to IF. Table 3 lists the main specifications of the interference monitoring equipment.

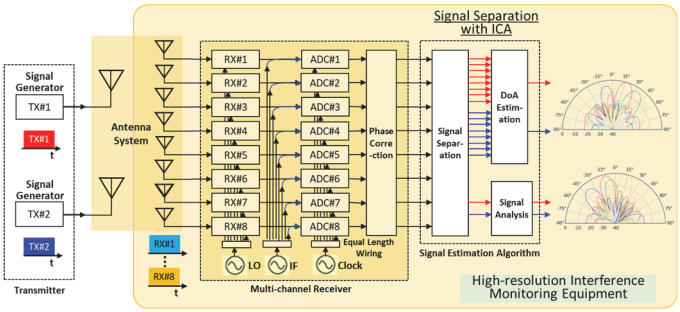

Figure 9 Interference Monitoring Equipment Configuration

Figure 10 External View of Interference Monitoring Equipment (Sub-6 GHz Band Measurement)

5 System Evaluation and Experiment

The prototyped error monitoring equipment was tested to evaluate the estimated DoA error and the Error Vector Magnitude (EVM) of separated signals.

Figure 11 shows the test antenna arrangement. The Rx array antenna had a maximum of 8 antennas arranged at a 1/2 wavelength interval. Each side had a dummy antenna terminated at 50Ω. These dummy antennas equalized the interconnect effect between the Rx antenna elements to improve the average effect, resulting in a reduced estimated arrival direction error over a wider area. The two Tx antennas (TX#1 and TX#2) were connected to the signal-source SG.

As shown in Figure 11 (b), the TX#1 antenna measurement was fixed at −10° and +10°, while the TX#2 antenna measurement was varied from −72° to +72°. Table 2 lists the main specifications of the Tx test signals. The Tx level was set so that the Tx level of TX#2 was −6 dB relative to TX#1.

Table 2 Live Tx Signal Test Items

Item	Sub-6 GHz Band	SHF Band
Center Frequency	3.75/4.65 GHz	28.25 GHz
Bandwidth	100 MHz	
Sub-carrier Spacing	30 kHz	120 kHz
No. of Slots	8	32
Resource Blocks	173	66
Encoding	QPSK	
Frequency Deviation	0	
Signal Sources	2	
No. of Rx Antennas	8	
No. of Carrier Paths	1	
Signal Tx Antenna	3.3 to 4.9 GHz Standard Gain Horn Antenna (A-Info) Gain: 10 dBi	WR-34 Pyramidal Horn Antenna (SAGE) Gain: 23 dBi

5.1 Amplitude and Phase Calibration

Since inter-channel amplitude and phase error have a large impact on the processing results, pre-measurement amplitude and phase calibration were used to minimize error factors.

The amplitude and phase calibration positioned one Tx antenna in the 0° direction as shown in Figure 11 (a) so the signal received at this time had equal amplitude and phase.

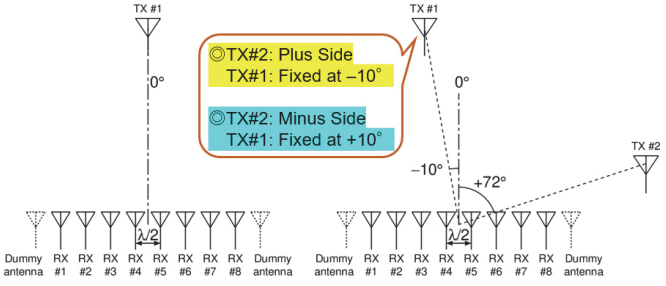

Figure 11 Live Test Antenna Arrangement

5.2 SHF-Band Live Test Results

Figure 12 shows the high-SHF band (28.25 GHz) test results with the separated signal estimated arrival direction error and angle spectrum in Figures 12 (a) and 12 (b), respectively. There were three test conditions: 1. Without calibration, 2. With only phase calibration, and 3. With both amplitude and phase calibration.

When performing both phase and amplitude calibration, the results were broadly similar and the estimated arrival direction error was less than 5° when the Tx antenna angle was varied between −72° and +72° and satisfied the target value of less than ±10°. In addition, error in the range between −48° and +54° was almost flat at 0°. On the other hand, without calibration, the error in the ±72° range was more than 5°. The ±10° target value was met at the Tx antenna angle range of ±54° indicating the noticeable impact of calibration. Figures 12 (b) (2) phase calibration and (3) amplitude calibration show that the side lobes are reduced more by amplitude calibration.

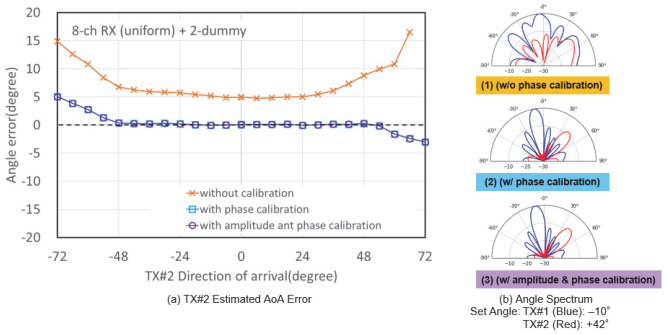

Figure 12 SHF-Band Estimated DoA Error

Figures 13 (a) and (b) show the EVM for TX#1 and TX#2 after signal separation. While the Tx level difference is not 6 dB, although there is no SNR limit, we think there is sufficient signal separation of at least 30 dB. Since Rx power drops due to antenna directivity as the DoA increases, the TX#2 EVM shows a tendency to increase. Although the dispersion at each EVM measurement becomes larger due to Sub-6 GHz band EVM characteristics described later (Figure 13), we think this is due to the large effect of phase noise in the high-SHF band.

The EVM results after separation (Figure 13) are shown in the following three cases:

1. When 8ch, 6ch, and 4ch received
2. When weighting applied to each Rx antenna so angle resolution equivalent to 6ch when receiving 8ch
3. When weighting applied so angle resolution equivalent to 4ch when receiving 6ch

Based on the waveform angle spectrum in Figure 13 (c), although weighting degrades the angular resolution, the side lobes are reduced. While this weighting processing restricts the angular range, it is effective in limiting the fake spectrum impact.

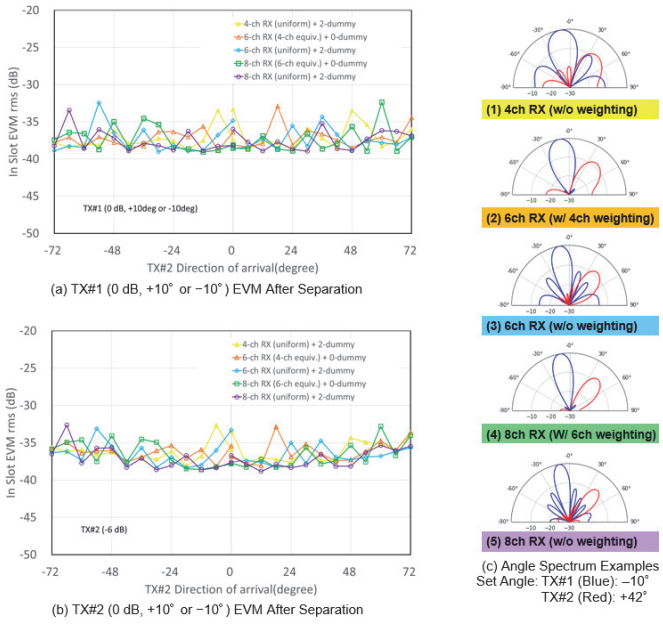

Figure 13 SHF-Band EVM Properties after Signal Separation

5.3 Sub-6 GHz Band Live Test Results

The test results for the high-SHF band (28.25 GHz) and the Sub-6 GHz (3.75 GHz) band in Figure 12 are shown in Figure 14. At every calibration condition, the estimated error was less than ±5° and satisfied the target error of ±10°. The characteristics were more or less flat in the ±54° range. Based on the angle spectrum in Figure 14 (b) (2) and (3), amplitude calibration was more effective at reducing sidelobes than only phase calibration. In comparison with the high SHF band results (Figure 12), the estimated error without calibration was smaller for the Sub-6 GHz band. This is thought to be because the inter-channel phase error is smaller because the frequency band is about 1/7 lower. In comparison with the angle spectrum in Figure 12 (b) (1) and Figure 14 (b) (1), although several ghost spectrum were observed in the high-SHF band, the Sub-6 GHz side lobes were mismatched.

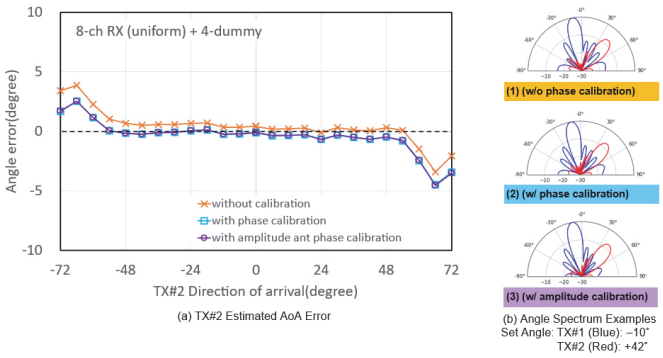

Figure 14 Sub-6 GHz Band Estimated DoA Error

Figures 15 (a) and (b) show the test results for the Sub-6 GHz band EVM characteristics after signal separation and Figure 15 (c) shows the angle spectrum waveform. Since the TX#2 Rx power drops due to the effect of array antenna directivity as the AoA becomes large, the TX#2 EVM increases slightly. The EVM increase near the 0° AoA is due to the difficulty of separating two signal sources with a small angular difference. Since the angular resolution decreases when weighting is applied to 6ch and 4ch, the respective EVM values are slightly degraded. Despite the above-observed trend, the target standards were met and the signals can be separated.

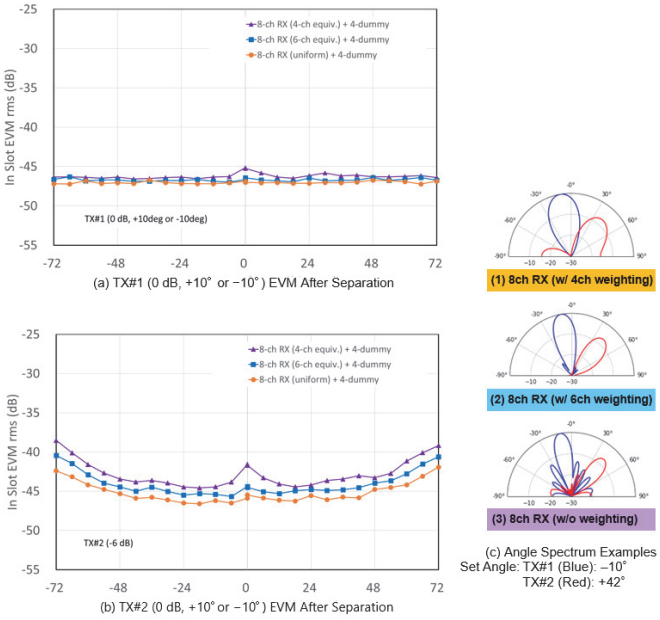

Figure 15 Sub-6 GHz EVM Properties after Signal Separation

6 Conclusion

We prototyped and evaluated interference monitoring equipment for separating blind signals in two frequency bands: 1. the high-SHF band (28 GHz), and 2. the Sub-6 GHz band (3.7 and 4.5 GHz). Although there were some differences in the range of the estimated arrival direction angle, we confirmed that the interference data required to obtain the IUI could be measured. Although this work evaluated the system under only a limited range of conditions, including the communications environment and conditions, frame pattern, etc., we obtained satisfied results to see possibility of using this interference monitoring method.

Future research will target testing and evaluation in wider various environments and conditions with feedback of

results to improve measurement accuracy and processing speed intended at actual usage in a real communications environment.

7 Acknowledgments

This research is supported by the Ministry of Internal Affairs and Communications (MIC) in Japan (JPJ000254). We thank the related R&D committee members for their valuable opinions and discussion during this research.

Table 3 Main Interference Monitoring Equipment Specifications

Item	Specification	
RF Section		
	Sub-6 GHz Band	SHF Band
Frequency	3.6 to 4.1 GHz 4.4 to 4.9 GHz	27.5 to 29.5 GHz
Input Level	−10 to −60 dBm (avg. power)	
IF Signal Output	369 ±100 MHz	
Intermodulation (IM3)	<−60 dBc (IF signal avg. power: at −7 dBm)	
S/N Ratio	>125 dBc/Hz	>120 dBc/Hz
	(Ratio of signal average power to noise power per 1 Hz at min RF input average power of −40 dBm)	
Digital Section		
Sampling Frequency	983.04 MHz	
I/Q Signal Bandwidth	100 MHz	
DDC Output	245.76 M Sample/s	
ADC Resolution	14-bit	

References

1) 3GPP, TS 36.211 v17.4.0 (2021-12), “Evolved Universal Terrestrial Radio Access (E-UTRA); Physical channels and modulation”
2) 3GPP, TS 38.101-2 v17.4.0 (2021-12), “User Equipment (UE) radio transmission and reception; Part 2: Range 2 Standalone”
3) 3GPP, TS 38. 211 v16.10.0 (2021-12), “NR; Physical channels and modulation”
4) “IEICE: Antenna Engineering Handbook, 2nd edition, Ohmsha, Ltd.,-2008
5) N. Kikuma, Fundamentals of Array Antennas, 2009 Microwave Exhibition Workshops and Exhibition, Tutorial 3 (2009-11-26)
6) M. Itami, “Easy-to-understand OFDM technology”, Ohmsha, Ltd., (2005) (in Japanese)
7) H. Arai, “Small antennas: miniaturization method and its evaluation method”, IEICE trans. commun. (Japanese edition), Vol. J87.B, No. 9, pp. 1140-1148 (2004-9) (in Japanese)
8) T. Fukasawa, H. Miyashita, H. Ohashi, Y. Konishi, “Characteristics of a Dipole Antenna on a Cell Phone without a Balun”, IEICE trans. commun. (Japanese edition), Vol. J92.B No. 9 pp. 1391-1398, (2009-9)
9) S. Adachi, T. Yoneyama, Electromagnetic wave transmission engineering, CORONA PUBLISHING CO., LTD. (Feb. 1981)
10) Aapo Hyvärinen, Juha Karhunen, Erkki Oja, Independent component analysis, Tokyo Denki University Press, 2005
11) R. Schmidt, “Multiple emitter location and signal parameter estimations”, Antennas Propag., Vol. 34, 3, pp. 276-280 (1986)
12) P. Smaragdis, “Blind separation of convolved mixtures in the frequency domain,” Neurocomput., vol. 22, pp. 21–34, 1998.
13) L. Sarperi, X. Zhu, and A. K. Nandi: “Blind OFDM Receiver Based on Independent Component Analysis for Multiple-Input Multiple-Output Systems”, IEEE Transactions on Wireless Communications, Vol. 6, 11, pp. 4079–4089 (2007)
14) T. Kim, H. T. Attias, S.-Y. Lee, and T.-W. Lee, “Blind Source Separation Exploiting Higher-Order Frequency Dependencies”, IEEE Transactions on Audio, Speech, and Language Processing, Vol. 15, 1, pp. 70–79 (2007)
15) S. Kurita, H. Saruwatari, S. Kajita, K. Takeda, and F. Itakura, “Evaluation of blind signal separation method using directivity pattern under reverberant conditions”, IEEE Int. Conf. Acoust. Speech Signal Proc. pp. 3140–3143 (2000)
16) J. Gao, X. Zhu, and A. K. Nandi, “LINEAR PRECODING AIDED BLIND EQUALIZATION WITH INDEPENDENT COMPONENT ANALYSIS IN MIMO OFDM SYSTEMS”, 16th European Sig. Process. Conf. (2008)
17) A. J. Bell and T. J. Sejowski “An information maximization approach to blind separation and blind deconvolution” Neural Networks, Vol. 10, No. 3, pp. 626-634 (1999)
18) A. Hyvarinen “Fast and Robust Fixed-Point Algorithms for Independent Component Analysis” IEEE Transactions on Neural Networks and Learning Systems, Vol 7, No 6, pp. 1129-1159 (1995)
19) H. Sawada, R. MUKAI, S, ARAKI, S, MAKINO “Polar Co-ordinate Based Nonlinear Function for Frequency-Domain Blind Source Separation” IEICE Transactions on Fundamentals of Electronics, Communications and Computer Sciences E86-A, No. 3 (2003)

20) E. Bingham and A. Hyvärinen, “A Fast Fixed Point Algorithm for Independent Component Analysis of Complex Valued Signals”, International Journal of Neural Systems, Vol. 10, 1, pp. 1 8 (2000)
21) N. Murata, S. Ikeda, and A. Ziehe, “An approach to blind source separation based on temporal structure of speech signals,” Neurocomputing, vol. 41, no. 1-4, pp. 1–24, 2001.
22) C.M Bishop, et, al. “Pattern Recognition and Machine Learning” (Japanese edition), Maruzen Publishing Co., Ltd., (2012)
23) U von Luxburg, “A tutorial on spectral clustering”, Statistics and Computing, Vol. 17, pp. 395 416 (2007)
24) scikit-learn, “Clustering”, https://scikit-learn.org/stable/modules/clustering.html
25) Roger A. Horn, Charles R. Johnson, “Matrix Analysis Second Edition,” Cambridge University Press, 2012.
26) T. Teshirogi and T. Yoneyama: Modern Millimeter-Wave Technologies, pp. 24-28, Ohmsha, Ltd., Tokyo, Japan (2001)
27) T. Fukushima, N. Michishita, H. Morishita, N. Fujimoto, “Broadband Sleeve Dipole Antenna with Consistent Gain in the Horizontal Direction”, IEICE Trans. on Commun., Vol.E101-B, No. 4, pp. 1061-1068 (2018-4)
28) Tibshirani, R., Walther, G., and Hastie, T.: Estimating the number of clusters in a data set via the gap statistic, Journal of the Royal Statistical Society B, Vol. 63, No. 2, pp. 411–423 (2001).
29) Jain, A.K. and Dubes, R.C.: Algorithms for clustering data, Englewood Cliffs, NJ: Prentice-Hall (1988).
30) Von Luxburg, U.: A Tutorial on Spectral Clustering, Statistics and Computing Journal. Vol. 17, Number 4, 2007, pp. 395–416.
31) “ADS54J64 Quad-Channel, 14-Bit, 1-GSPS, 2x Oversampling, Analog-to-Digital Converter Data Sheet (Initial release.)”, Texas Instruments, SBAS841, OCTOBER 2017
32) Y. Maruyama, N. Maekawa, M. Fuse, K. Shioiri, Blind OFDM Signal Separation using Frequency Domain ICA and K-means Clustering, 2020 IEICE Society Conference A-8-7 (Sep. 2020)
33) Y. Maruyama, N. Maekawa, M. Fuse, Investigation of Blind OFDM Signal Separation using Frequency Domain ICA and Spectral Clustering, The Institute of Electrical Engineers of Japan, Instrumentation and Measurement Study Group IM-21-008 (Jan. 2021)
34) Y. Maruyama, N. Maekawa, T. Kato Comparison of clustering methods as a means of resolving the permutation indeterminacy in OFDM signal separation with FDICAIEICE Technical Report, vol. 121, no. 393, SRW2021-66, pp. 7-9 (Mar. 2022)
35) Y. Maruyama, N. Maekawa, T. Kato Investigation of Single Linkage Clustering Method in Blind OFDM Signal Separation using Frequency Domain ICA., The Institute of Electrical Engineers of Japan, Instrumentation and Measurement Study Group IM-22-009 (3/11/2022)
36) “Signal Analyzer MS2850A Data Sheet”, ANRITSU CORPORATION ddcm/CDT No. MS2850A_Datasheet-J-A-1-(3.00) (3/13/2018)
37) “MX285051A-011/MX269051A-011 NR TDD sub-6GHz Downlink MX285051A-021 NR TDD mmWave Downlink MX285051A-061/MX269051A-061 NR TDD sub-6GHz Uplink MX285051A-071 NR TDD mmWave Uplink Operation Manual Operation”, ANRITSU CORPORATION 5th Edition, Document No.: M-W3963AE-5.0 (2/20/2019)
38) “Vector Signal Generator MG3710E Datasheet”, ANRITSU CORPORATION ddcm/CDT No. MG3710E_DataSheet-E-A-1-(1.00) (5/23/2019)
39) “MG3700A/MG3710A Vector Signal Generator [MG3740A Analog Signal Generator] Operation Manual (IQproducer™)”, ANRITSU CORPORATION 16th Edition Document No.: M-W2496AE-16.0 (5/13/2016)

Authors


Toyoyuki Kato
3rd laboratory
Advanced Research Laboratory


Takashi Mori
3rd laboratory
Advanced Research Laboratory


Masanori Takizawa
3rd laboratory
Advanced Research Laboratory


Takashi Kawamura
2nd Product Development Dept.
Product Development
Mobile Solutions Division
Test & Measurement Company


Yuici Maruyama
3rd laboratory
Advanced Research Laboratory

Publicly available